

Amide proton transfer (APT) magnetic resonance imaging of prostate cancer: comparison with Gleason scores

Yukihisa Takayama¹ · Akihiro Nishie² · Masaaki Sugimoto^{3,4} · Osamu Togao² · Yoshiki Asayama² · Kousei Ishigami² · Yasuhiro Ushijima² · Daisuke Okamoto² · Nobuhiro Fujita² · Akira Yokomizo⁴ · Jochen Keupp⁵ · Hiroshi Honda²

Received: 24 November 2015 / Revised: 11 February 2016 / Accepted: 12 February 2016 / Published online: 10 March 2016
© ESMRMB 2016

Abstract

Objective To evaluate the utility of amide proton transfer (APT) imaging in estimating the Gleason score (GS) of prostate cancer (Pca).

Materials and methods Sixty-six biopsy-proven cancers were categorized into four groups according to the GS: GS-6 (3 + 3); GS-7 (3 + 4/4 + 3); GS-8 (4 + 4) and GS-9 (4 + 5/5 + 4). APT signal intensities (APT SIs) and apparent diffusion coefficient (ADC) values of each GS group were compared by one-way analysis of variance with Tukey's HSD post hoc test.

Results The mean and standard deviation of the APT SIs (%) and ADC values ($\times 10^{-3}$ mm²/s) were as follows: GS-6, 2.48 \pm 0.59 and 1.16 \pm 0.26; GS-7, 5.17 \pm 0.66 and 0.92 \pm 0.18; GS-8, 2.56 \pm 0.85 and 0.86 \pm 0.17; GS-9, 1.96 \pm 0.75 and 0.85 \pm 0.18, respectively. The APT SI of the GS-7 group was highest, and there were significant differences between the GS-6 and GS-7 groups and the GS-7

and GS-9 groups ($p < 0.05$). The ADC value of the GS-6 group was significantly higher than each value of the GS-7, GS-8, and GS-9 groups ($p < 0.05$), but no significant differences were obtained among the GS-7, GS-8, and GS-9 groups.

Conclusion The mean APT SI in Pca with a GS of 7 was higher than that for the other GS groups.

Keywords Amide proton transfer · Apparent diffusion coefficient values · Prostate cancer · Gleason score

Introduction

Prostate cancer (Pca) is the most frequently diagnosed cancer in men, and it is the second most common cause of cancer death in men in the United States [1, 2]. It is thus important to assess the aggressiveness of Pca in order to determine an appropriate initial treatment strategy [3]. The Gleason grading system is the pathologic reference standard for measuring Pca aggressiveness [4–7]. Because an invasive needle biopsy or prostatectomy is necessary for obtaining the Gleason score (GS), a noninvasive measure of Pca aggressiveness is desirable.

Magnetic resonance imaging (MRI) can yield information on tumor aggressiveness using diffusion-weighted imaging (DWI), dynamic contrast-enhanced MRI (DCE-MRI) and MR spectroscopy [8–14]. Amide proton transfer (APT) has been introduced as a novel endogenous contrast mechanism for MRI through the detection of low-concentration solutes such as mobile proteins and peptides in tissues or tumors that contain abundant amide (–NH) chemical constituents [15, 16].

According to previous reports of APT imaging of brain tumors, high-grade gliomas show high APT signal

✉ Akihiro Nishie
anishie@radiol.med.kyushu-u.ac.jp

¹ Department of Radiology Informatics and Network, Graduate School of Medical Sciences, Kyushu University, 3-1-1 Maidashi, Higashi-ku, Fukuoka 8128582, Japan

² Department of Clinical Radiology, Graduate School of Medical Sciences, Kyushu University, 3-1-1 Maidashi, Higashi-ku, Fukuoka 8128582, Japan

³ Department of Anatomic Pathology, Graduate School of Medical Sciences, Kyushu University, 3-1-1 Maidashi, Higashi-ku, Fukuoka 8128582, Japan

⁴ Department of Urology, Graduate School of Medical Sciences, Kyushu University, Fukuoka, 3-1-1 Maidashi, Higashi-ku, Fukuoka 8128582, Japan

⁵ Philips Research, Roentgenstr. 24-26, 22335 Hamburg, Germany

intensity (APT SI), and low-grade gliomas show low APT SI. The authors of these reports thus concluded that APT imaging is useful for assessing tumor aggressiveness [15, 17]. Although most clinical studies of APT imaging have involved neuroimaging [15, 17], a few studies have reported on APT imaging of breast cancer and Pca [18, 19]. In an APT imaging study of Pca, the APT SI was used to differentiate Pca from noncancerous tissue in the peripheral zone (PZ) [19]. However, the utility of this imaging method for assessing the GS of Pca remains unclear. The purpose of the present study was to evaluate the utility of APT

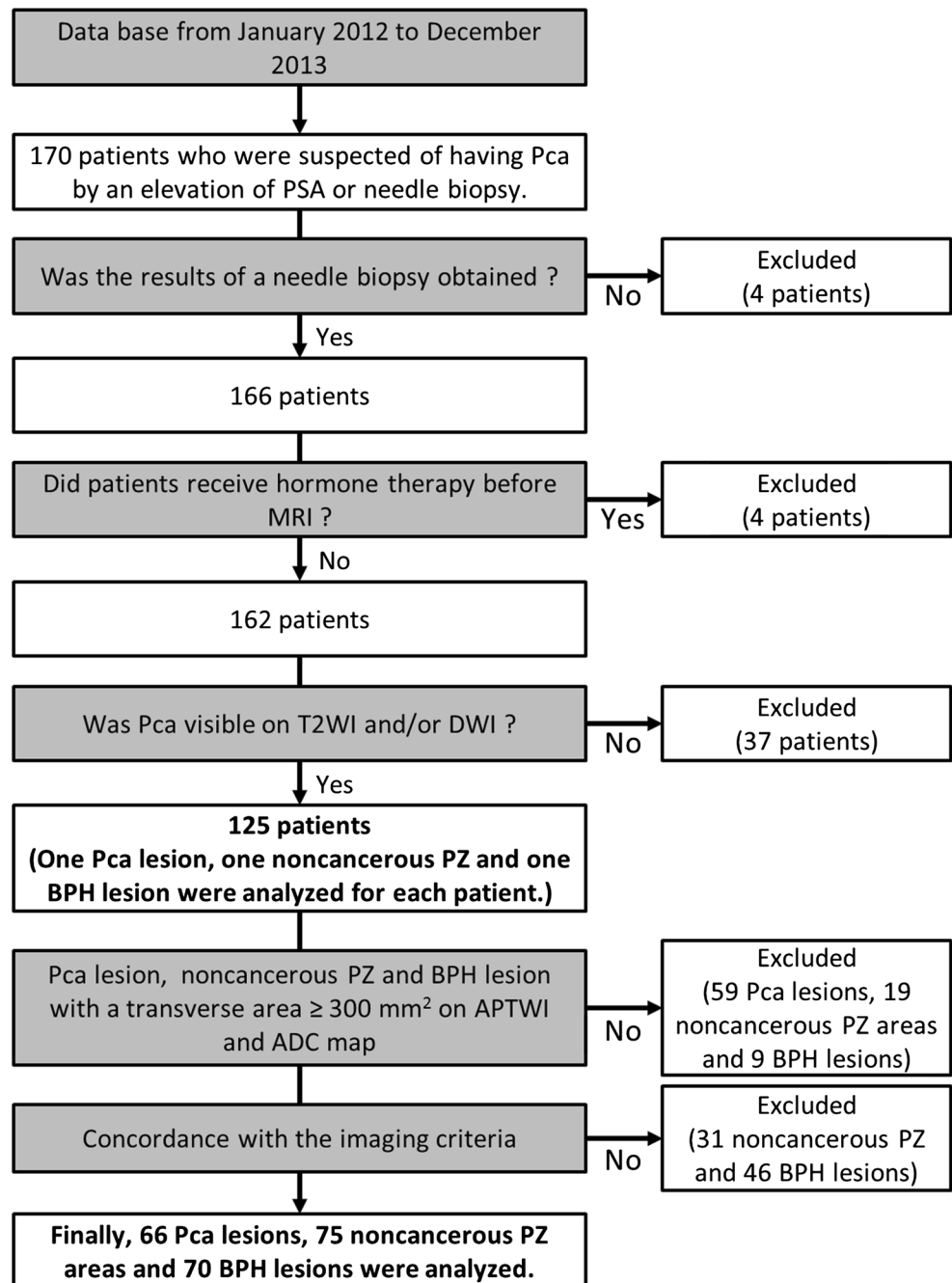
imaging in assessing the GS of Pca through radiological-pathological comparison.

Materials and methods

Patients

From January 2012 to December 2013, 170 consecutive male patients were scheduled for MR examinations for suspected Pca based on elevated prostate-specific antigen

Fig. 1 Patient selection flow-chart. Imaging criteria of Pca lesion, noncancerous PZ and BPH lesion are described in the data analysis of the APT imaging and the DWI/ADC map in the “Materials and methods” section



(PSA) levels or needle biopsy results. A summary flowchart of the patient selection is presented in Fig. 1. A total of 125 patients (mean age 68.4 years, range 50–80 years) were included in the analysis. The mean (range) serum PSA level among the 125 patients was 14.9 (0.01–291.3) ng/mL. Fifteen patients underwent the MR examination before needle biopsies, and the other 110 underwent the MR examination at least 8 weeks after a needle biopsy to minimize the possible interference of post-biopsy hemorrhage in the accurate detection of Pca [20].

MRI

MR examinations were performed on a clinical whole-body 3.0 Tesla MRI system equipped with a dual-source parallel radiofrequency (RF) subsystem for transmission via a two-channel RF body coil (Achieva 3.0T TX; Philips Healthcare, Best, The Netherlands). A 32-channel torso-cardiac coil was used for parallel imaging. In addition to other MRI including T1-weighted imaging (T1WI), T2-weighted imaging (T2WI), DWI and DCE-MRI, APT imaging was performed prior to DCE-MRI. APT imaging was obtained in the transverse plane. T2WI, DWI and DCE-MRI were used for the localization of Pca and/or noncancerous regions.

The acquisition software was modified to alternate the operation of the two transmission RF sources during the RF saturation pulse, which enables long quasi-continuous RF saturation at a 100 % RF duty cycle. Special RF shimming

for the saturation homogeneity of the alternated pulse was applied, adjusting the RF amplitudes of the two transmission RF sources to equalize the B_1 -field [17, 21]. On a single slice corresponding to a maximum cross-section area of a tumor, two-dimensional (2D) transverse APT imaging was performed using a saturation pulse with a duration (T_{sat}) of 0.5 s (10×50 ms, sinc-Gauss-shaped elements) and a saturation power level corresponding to $B_{1,\text{rms}} = 2.0 \mu\text{T}$. During each MR examination, a single slice on which a tumor appeared to be present was selected by an experienced radiologist, as referring to other MRI. For the acquisition of an APT Z-spectrum, imaging was repeated at 25 saturation frequency offsets from $\omega = -6.0$ to $+6.0$ ppm in 0.5-ppm increments, as well as one far off the resonant frequency ($\omega = -1560.0$ ppm) for signal normalization. In addition to B_0 shimming before the scan, a ΔB_0 map for off-resonance correction was acquired separately using a 2D dual gradient-echo sequence ($\Delta\text{TE} = 1$ ms) with identical spatial resolution, which was used for a point-by-point ΔB_0 correction. The other MR parameters of the APT imaging and MR parameters of T1WI, T2WI, DWI and DCE-MRI are summarized in Table 1. An apparent diffusion coefficient (ADC) map was generated with reference to the signal intensities of DWI with b values of 0 and 1000 s/mm^2 .

Histopathological analysis

The needle biopsy was performed at 12 different sites of the prostate for each patient. Pathological examinations

Table 1 Details of MR parameters

	APT imaging	T1WI	T2WI	DWI	DCE-MRI
Imaging technique	2D single-shot TSE	2D GRE	2D TSE	2D single-shot EPI	3D GRE
TR/TE (ms)	5000/6	150/2.3	5000/90	5000/64	2.9/1.6
Flip angle ($^\circ$)	90	75	90	90	10
Field of view (mm^2)	230×230	150×150	200×200	300×300	250×250
Matrix (frequency \times phase)	128×128	150×150	400×320	96×80	160×151
Slice thickness (mm)	5	3	4	4	1
Slice gap (mm)	N/A	0	1.5	1.5	N/A
Number of slices	1	30	20	20	80
Number of excitations	1	1	1	2	1
ETL (TSE factor)	128	N/A	17	N/A	43
EPI factor	N/A	N/A	N/A	31	N/A
SENSE factor	2	1	1	3	1
b value, s/mm^2	N/A	N/A	N/A	0, 1000 and 2000	N/A
Respiratory compensation	Free-breathing	Free-breathing	Free-breathing	Free-breathing	Free-breathing
Fat suppression	N/A	N/A	N/A	SPAIR	SPAIR
Total scan time (min:sec)	2:20	1:00	3:52	3:15	1:40 (0:09 for each phase)

APT amide proton transfer, T1WI T1-weighted imaging, T2WI T2-weighted imaging, DWI diffusion-weighted imaging, DCE-MRI dynamic contrast-enhanced magnetic resonance imaging, TSE turbo spin echo, GRE gradient echo, EPI echo planar imaging, TR repetition time, TE echo time, ETL echo train length, SENSE sensitivity encoding, SPAIR spectral attenuation with inversion recovery, N/A not applicable

were reviewed by one pathologist (M.S., 8 years of experience in the examination of Pca). First, the presence/absence of cancer tissue at each biopsy site was recorded. Pca was then categorized into one of four GS groups as follows: GS-6 (3 + 3), GS-7 (3 + 4 or 4 + 3), GS-8 (4 + 4) or GS-9 (4 + 5 or 5 + 4).

Data analysis of the APT imaging and the DWI/ADC map

Two experienced radiologists (A.N. and Y.T., 20 and 14 years of experience in interpreting Pca, respectively) reviewed all of the MR images in consensus. In this study, because the APT imaging was of a single slice, one Pca lesion, one noncancerous PZ and one benign prostate hyperplasia (BPH) lesion were analyzed for each patient (Table 1). For patients with multiple Pca lesions, the largest Pca lesion was selected for analysis. First, the two radiologists identified nodules showing no high intensity on T1WI, low intensity on T2WI, high intensity on DWI with b values of 1000 and/or 2000 s/mm², low ADC and early enhancement on DCE-MRI results for the same slice location as that used for the APT imaging. Second, they confirmed whether these nodules were located at the site of Pca based on the histopathological data obtained by the needle biopsy.

In addition to Pca lesions, noncancerous PZ and BPH lesions were included in the analysis to enable a comparison between benign and malignant lesions. Even if there were multiple areas of noncancerous PZ and BPH lesions were existed in each patient, one noncancerous PZ and one BPH lesion, which showed the largest area on the same image slice of Pca, were selected for the analysis. Areas of noncancerous PZ were defined as high SI on T2WI, low SI on T1WI and DWI with b values of 1000 and 2000 s/mm² compared with noncancerous PZ, and they confirmed the absence of Pca by using the needle biopsy results. The area of BPH was defined as high or mixed high and low SI on T2WI, low SI on T1WI and DWI with b values of 1000 and 2000 s/mm², and the absence of Pca was confirmed using the needle biopsy results.

We analyzed the APT imaging data with ImageJ software (National Institutes of Health, Baltimore, MD, USA), using a custom-made plug-in for APT imaging. The analysis method was reported in a previous study [17]. The plug-in was created to assess the Z-spectra and magnetization transfer ratio asymmetry (MTR_{asym}), and was equipped with a correction function for B_0 inhomogeneity, using interpolation among the Z-spectral images. First, rigid-body motion correction was performed using the TurboReg algorithm. The local B_0 field shift in Hz was obtained from the B_0 map, which was created from dual gradient-echo images (TE1 and 2) according to the following equation:

$$\Delta B_0(\times) = (\text{Phase}[\text{TE2}](\times) - \text{Phase}[\text{TE1}](\times)) / (\text{TE2} - \text{TE1}) * 2 * \text{Pi}$$

where phase [TEi](\times) indicates phases of the images with echo times TE1 or TE2 at position \times in radians, and TE1 and TE2 are given in seconds. The $\Delta B_0(\times)$ is the resulting B_0 map measured in Hz. The image intensity of each voxel was corrected for the nominal saturation frequency offset by Lagrange interpolation among the neighboring Z-spectral images. This procedure corresponds to a frequency shift along the saturation frequency offset axis according to the measured B_0 shift.

The MTR was defined as $1 - S_{\text{sat}}/S_0$, where S_{sat} and S_0 are the SIs obtained with and without selective saturation, respectively. The analysis method was reported in a previous study [16]. To reduce the unwanted contributions from the conventional magnetization transfer (MT) effect and the direct saturation of bulk water, we performed an asymmetry analysis of MTR values with respect to the water frequency. For the APT imaging, the asymmetry analysis at 3.5 ppm downfield from the water signal was calculated as $MTR_{\text{asym}}(3.5 \text{ ppm})$:

$$\begin{aligned} MTR_{\text{asym}}(3.5 \text{ ppm}) &= [S_{\text{sat}}(3.5 \text{ ppm}) - S_{\text{sat}}(+3.5 \text{ ppm})] / S_0 \\ &= MTR'_{\text{asym}}(3.5 \text{ ppm}) \end{aligned}$$

where MTR'_{asym} is the inherent asymmetry of the conventional MT effect, and APTR is the amide proton transfer ratio [16]. Thus, it should be noted that the measured $MTR_{\text{asym}}(3.5 \text{ ppm})$ values are the apparent APT SIs, and thus it is appropriate to define the calculated $MTR_{\text{asym}}(3.5 \text{ ppm})$ images as APT-weighted imaging (APTWI). In the present study, APT SI was defined as $MTR_{\text{asym}}(3.5 \text{ ppm}) \times 100 (\%)$.

The ADC values were calculated on a commercially available PACS workstation (SYNAPSE, Fujifilm Medical Co., Ltd., Tokyo, Japan). The means and standard deviations (SDs) of the APT SIs or ADC values of Pca, noncancerous PZ and BPH were measured by drawing polygonal regions of interest (ROIs) on source images of APTWI and placing these ROIs on the same slice of the ADC map by consensus of the two readers. When the ROIs of the tumor in the noncancerous PZ or BPH were drawn on the APTWI and ADC maps, as much tumor as possible was included, referring to information from the T2WI, DWI and DCE-MRI. To minimize the effect of noise on the measurement of APT SIs and ADC values, only tumors with a transverse area $\geq 300 \text{ mm}^2$ on APTWI and ADC maps (≥ 93 pixels on APTWI) were included for the analysis. The mean (range) area among analyzed Pca was 651.7 (306.7–3080.2) mm². Similarly, only noncancerous PZ and BPH with an area $\geq 300 \text{ mm}^2$ were included. The mean (range) areas of analyzed noncancerous PZ and BPH were 577.2 (306.7–2531.3) mm² and 990.3 (326.1–3512.9) mm², respectively.

Statistical analysis

The mean APT SIs and ADC values of the Pca, noncancerous PZ and BPH were compared by one-way analysis of variance (ANOVA) with Tukey's honest significant difference (HSD) post hoc test. Spearman's rank correlation coefficients (Spearman's ρ) were calculated between the APT SI and GS groups and between ADC values and GS groups. All statistical analyses were performed with PASW Statistics for Windows, Version 18.0 (SPSS Inc., Chicago, IL, USA). Values of $p < 0.05$ were considered significant for each analysis.

Results

Numbers of analyzed tumor and noncancerous regions

Fifty-nine Pca lesions, 19 noncancerous PZ areas and nine BPH lesions were excluded due to small size ($< 300 \text{ mm}^2$; < 93 pixels) on APTWI. Thirty-one noncancerous PZ and 46 BPH lesions were excluded due to discordance with the imaging criteria described in "Materials and methods." Ultimately, 66 Pca lesions, 75 noncancerous PZ areas and 70 BPH lesions were analyzed (Fig. 1). The 66 Pca lesions were categorized into four GS groups as follows: GS-6 ($n = 23$ lesions), GS-7 ($n = 18$), GS-8 ($n = 11$) and GS-9 ($n = 14$). No Pca with a GS less than 6 or greater than 9 was present in our population. Among the total 66 Pca lesions, 33, 10 and 23 were located in the PZ, transitional zone (TZ) and both PZ and TZ, respectively.

APT SIs and ADC values among the four GS groups

The results of APT SI comparisons among the four GS groups are shown in Fig. 2. Of these, GS-7 showed the highest APT SIs ($5.17 \pm 2.89 \%$) and GS-9 showed the lowest ($1.96 \pm 2.42 \%$). There were significant differences between the GS-6 and GS-7 groups and between the GS-7 and GS-9 groups ($p < 0.05$), but there were no significant differences between the GS-6 and GS-8 groups, the GS-6 and GS-9 groups, or the GS-7 and GS-8 groups.

The results of the comparison of ADC values among the four GS groups are shown in Fig. 3. There were significant differences between the GS-6 and GS-7 groups, the GS-6 and GS-8 groups, and the GS-7 and GS-9 groups ($p < 0.05$), but there were no significant differences between any two of the GS-7, GS-8, and GS-9 groups.

APT SIs and ADC values between noncancerous regions and prostate cancer

Comparisons of APT SIs among the noncancerous PZ regions, BPH and each GS group are shown in Fig. 2. There

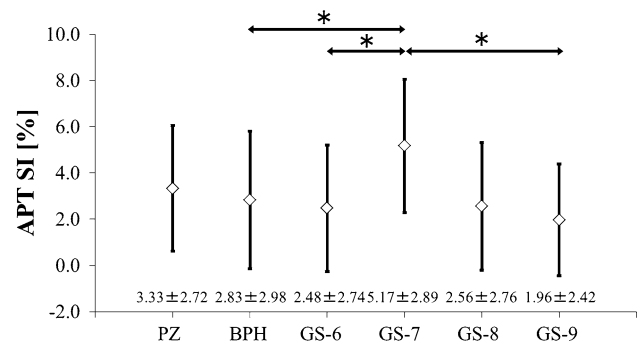


Fig. 2 Means and SDs of the APT SIs of each GS group of prostate cancer lesions, noncancerous peripheral zone (PZ) areas and benign prostate hyperplasia (BPH) lesions. The unit of APT SI is percentage. The GS-7 group showed the highest APT SIs among the four groups. There were significant differences between the GS-6 and GS-7 groups and the GS-7 and GS-9 groups. There was a significant difference between the BPH and GS-7 groups, but no significant differences between the noncancerous PZ and each of the GS groups. $*p < 0.05$ by one-way ANOVA and Tukey's HSD test

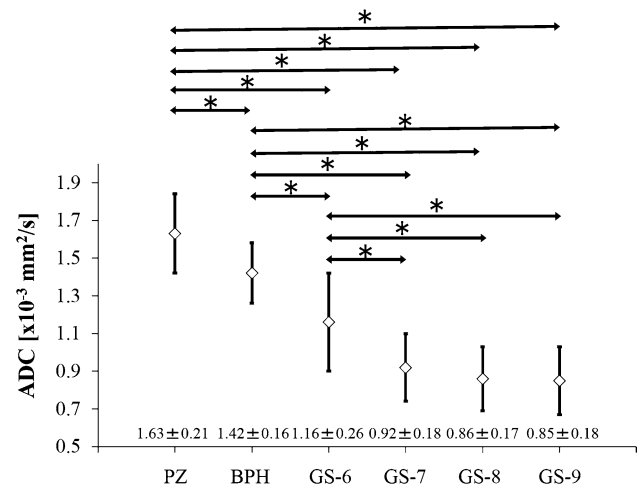
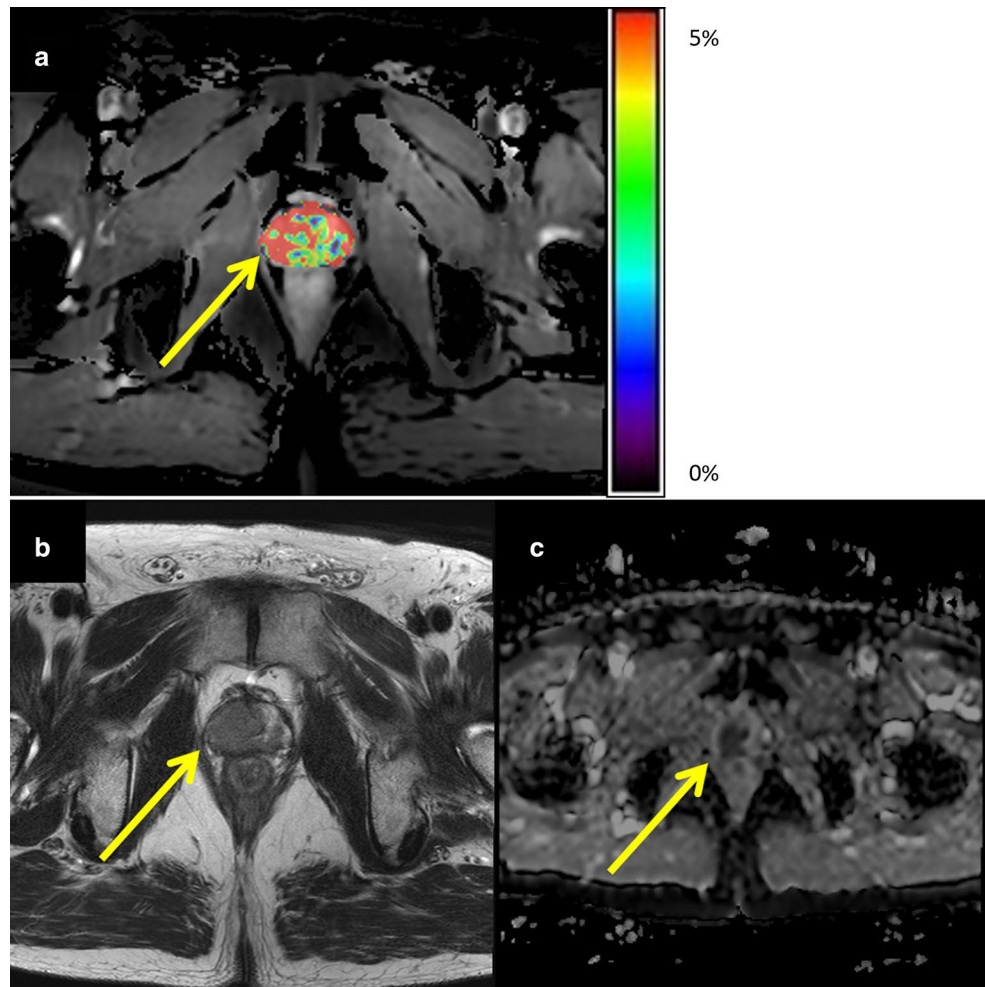


Fig. 3 Means and SDs of the ADC values of each GS group of prostate cancer, noncancerous PZ areas and BPH lesions. The unit of ADC value is $\times 10^{-3} \text{ mm}^2/\text{s}$. There was a significant difference between the noncancerous PZ and BPH values and between the noncancerous PZ areas and each GS group. There were also significant differences between the BPH and each of the GS groups. $*p < 0.05$ by one-way ANOVA and Tukey's HSD test

was a significant difference between BPH ($2.83 \pm 2.98 \%$) and the GS-7 group ($p < 0.05$), but there were no significant differences between the noncancerous PZ areas ($3.33 \pm 2.72 \%$) and any of the GS groups.

Comparisons of ADC values among the noncancerous PZ areas, BPH and each GS group are shown in Fig. 3. There were significant differences between the noncancerous PZ group and each GS group and between the BPH group and each GS group ($p < 0.05$). There were also significant differences between the noncancerous PZ areas and the BPH

Fig. 4 A 54-year-old man with GS-7 prostate cancer. **a** APT-weighted image of the prostate fused with a fat-suppressed proton density-weighted image; **b** T2-weighted image; **c** ADC map. The tumor was located in the right lobe of the PZ. The tumor showed APT SI of 5.4 % and ADC value of $0.68 \times 10^{-3} \text{ mm}^2/\text{s}$



group ($p < 0.05$). Example cases of Pca lesions with GS-7 and GS-9 are shown in Figs. 4 and 5, respectively.

Rank correlations between the APT SIs and GS groups and between the ADC values and GS groups

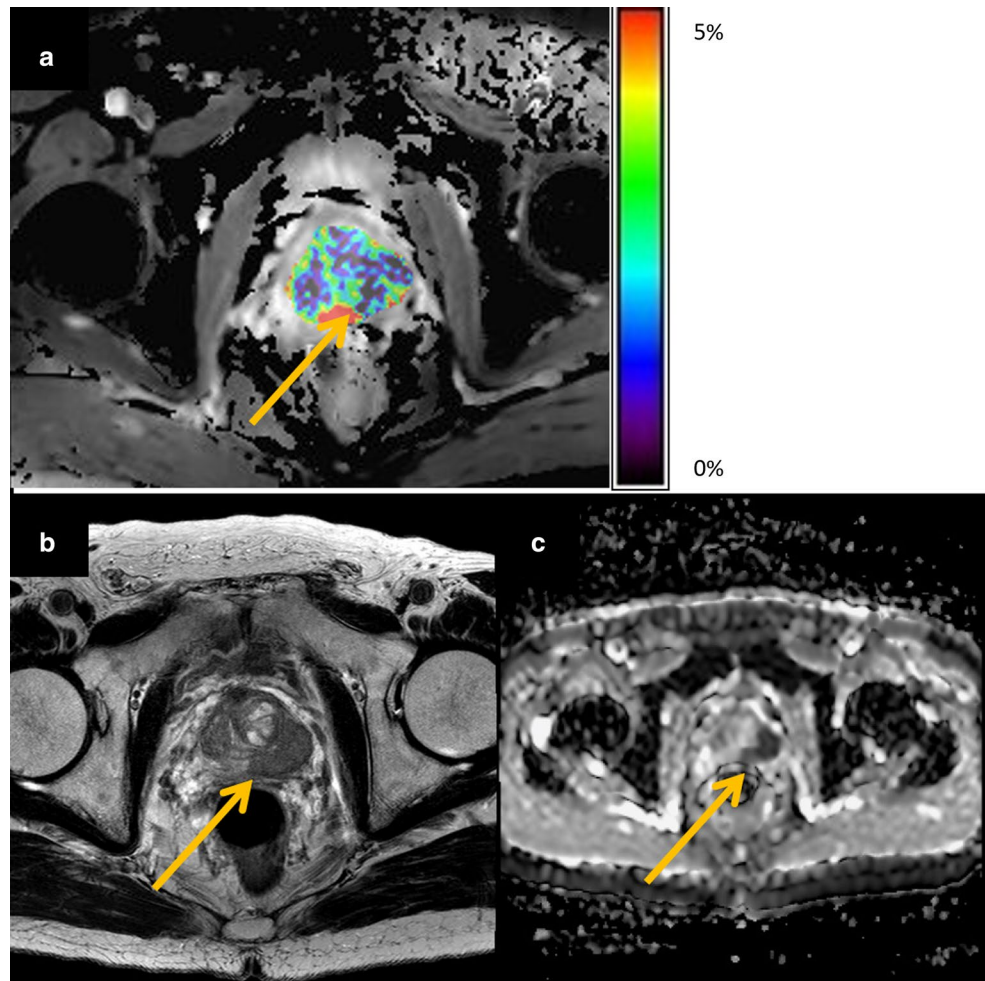
There was no significant correlation between APT SIs and GS groups (Spearman's $\rho = -0.043$, $p = 0.53$), but there was a significant correlation between the ADC values and GS groups (Spearman's $\rho = -0.795$, $p < 0.01$).

Discussion

Pca lesions from the GS-7 group, which are categorized as intermediate-risk Pca, showed the highest APT SIs among the four GS groups. However, the APT SIs did not show a significant rank correlation with the GS groups. The results of the present study differ from those involving APT imaging of brain tumors [15, 17]. The relevant literature reveals that aggressive malignant tumors (e.g.,

high-grade gliomas) show high APT SIs, and less aggressive malignant tumors (e.g., low-grade gliomas) show low APT SIs. The APT signals of brain tumors are positively correlated with cellular density and/or proliferation, i.e., intracellular mobile proteins and peptides [15, 17]. A study using APT imaging of Pca showed that APT SIs for GS-8 Pca (1.44 %), which was the APT SI calculated from one tumor, were smaller than for GS-7 lesions (6.4 ± 2.6 % in 3 + 4, 6.0 ± 3.7 % in 4 + 3). The results of our study were consistent with those of a previous study using APT imaging of Pca, even though the saturation schemes differed between the present study ($T_{\text{sat}} = 0.5$ s and $B_{1,\text{rms}} = 2.0$ μT) and the previous study ($T_{\text{sat}} = 0.496$ s and $B_{1,\text{rms}} = 3.8$ μT) [19]. Another study suggested that $T_{\text{sat}} = 0.6$ s and $B_{1,\text{rms}} = 2.0$ μT were optimal for obtaining APT MRI contrast between Pca lesions and noncancerous PZ areas [22]. Although there was a difference in T_{sat} between the present and previous studies, the duration and power of the saturation RF powers in the present study might be appropriate for the assessment of APT SIs in Pca [22].

Fig. 5 A 65-year-old man with GS-9 prostate cancer. **a** APT-weighted image of the prostate fused with a fat-suppressed proton density-weighted image; **b** T2-weighted image; **c** ADC map. The tumor was located in the left lobe of the PZ. The tumor showed APT SI of 2.2 % and ADC value of $0.62 \times 10^{-3} \text{ mm}^2/\text{s}$



With regard to the relationship between the ADC values of the present Pca and GS groups, our results showed a significant negative correlation, which is consistent with previous findings [8, 12, 23–27]. The reduction in ADC values in malignant tumors is related to histopathological characteristics, such as cellular density and the percentage area of nuclei and cytoplasm, resulting in a restriction of the movement of water molecules [8, 28–31]. In addition, it is reported that there is a positive correlation between ADC and the percentage area of luminal space for Pca [8, 29, 30, 32]. That is, the ADC values of Pca decreased and the tumor cellularity of the prostate increased in accordance with Pca aggressiveness. The APT SIs and ADC values in the present study showed different changes even though those two indices are considered to be related to cellular density [8, 17, 28–30, 32]. We hypothesized that other factors except for cellular density may also affect the APT SI in Pca.

The Gleason grading system, which is commonly used for evaluating Pca [5, 33], consists of two digits that signify the primary and secondary patterns in Pca, based on a scale of 1 (least aggressive) to 5 (most aggressive) [5, 33].

In normal prostate tissue, the glands are typically large, with an arbitrary shape, and contain abundant nuclei on the boundary [5]. The normal prostate gland comprises a network of water-rich ducts and acini supported by stroma [29]. The stroma is much looser in the PZ than in the central gland, resulting in a larger extracellular space [29]. PZ tissue contains numerous glands, and the glandular cavity is full of liquids and mobile proteins and peptides [29]. Gleason pattern 3 cancer consists of discrete glandular units, typically with smaller glands than those seen in Gleason pattern 1 or 2 cancers, in addition to infiltrates in and among non-neoplastic prostate acini, marked variations in size and shape, and smoothly circumscribed small cribriform tumor nodules [5]. Glands of Gleason pattern 4 cancer tend to be fused together rather than isolated as those in Gleason pattern 3 [34]. Gleason pattern 4 cancer consists of fused microacinar glands, ill-defined glands with poorly formed glandular lumina, large cribriform glands, cribriform glands with an irregular border, and a hypernephromatoid pattern [5]. Gleason pattern 5 cancer shows essentially no glandular differentiation, and it is composed of solid sheets, cords, or single cells, and comedocarcinoma

with central necrosis surrounded by papillary, cribriform or solid masses [5, 34]. As the prostate gland contains liquid and soluble proteins, we hypothesize that the change in glandular structures, i.e., extracellular mobile proteins and peptides, might affect the APT SI of the GS groups [29].

The higher APT SI of the GS-7 group may be the result of two counteracting effects. With regard to the comparison among noncancerous PZ and Pca with GS-6 and GS-7, the cellular density of Pca increases in accordance with the progression of GS [28–30, 32]. On the other hand, glandular structures containing liquids and mobile proteins and peptides still exist in Pca with GS-6 and GS-7. Contrarily, the cellular density in Pca with GS-8 or GS-9 is increased compared to GS-7, but the number of glandular structures is decreased. We speculate that the decrease in the number of glandular structures reduces the amount of liquids and mobile proteins and peptides. If we consider that APT SI may be affected by both cellular density (“intracellular” mobile proteins and peptides) and glandular structures (“extracellular” mobile proteins and peptides), the higher APT SI in the GS-7 group may be explained by a particular balance between the contributions of these two phenomena.

One major limitation of this study is that the histopathological results for the Gleason scores were obtained from needle biopsies. Needle biopsies have been shown to lead to a 25–69 % underestimation of GS compared with GS established from prostatectomy specimens, as sampling errors are occasionally unavoidable due to the histological heterogeneity of Pca [11, 26, 35]. Therefore, there is a risk of underestimating true Pca aggressiveness using our methodology. However, it was difficult for us to collect a sufficient number of patients with a highly aggressive Pca who had undergone a prostatectomy without prior hormone therapy and/or radiotherapy.

There were other drawbacks in the study. First, because of time limitations for the imaging protocol, APT imaging is limited to one slice per patient. In this study, only the largest Pca lesion was selected in patients with multiple Pca lesions, as assessment of the entire prostate gland was deemed impossible. In addition, the spatial resolution of the APT imaging was $1.8 \times 1.8 \times 5.0 \text{ mm}^3$, making it difficult to assess small Pca lesions. We also did not compare APT imaging with other multi-parametric MR techniques such as DCE-MRI and MR spectroscopy. These imaging techniques are known to be useful as noninvasive means of estimating Pca aggressiveness. Another study limitation was that we could not divide the GS-7 tumors into two groups of GS 3 + 4 and GS 4 + 3, and the GS-9 tumors into two groups of GS 4 + 5 and GS 5 + 4. According to the literature, the prognosis of patients with a GS of 4 + 3 is worse than that of patients with a GS of 3 + 4 [36], but there were insufficient numbers of Pca lesions in the present study for such comparisons.

Conclusions

The mean APT SI in Pca with a GS of 7 was higher than that for the other GS groups, but the APT SIs did not show significant rank correlation with GS groups.

Acknowledgments This work was supported by a Grant-in-Aid for Scientific Research (C), JSPS KAKENHI Grant Number 25461833.

Compliance with ethical standards

Conflict of interest Jochen Keupp declares that he receives a salary from Philips Research. The other authors have no conflict of interest.

Ethical standards This prospective study was approved by our institutional review board and complied with ethics committee standards. All procedures performed in studies involving human participants were in accordance with the ethical standards of the institutional research committee and with the 1964 Helsinki declaration and its later amendments or comparable ethical standards.

Informed consent Written informed consent was obtained from all individual participants included in the study.

References

1. Damber JE, Aus G (2008) Prostate cancer. *Lancet* 371:1710–1721
2. Siegel R, Naishadham D, Jemal A (2012) Cancer statistics, 2012. *CA Cancer J Clin* 62:10–29
3. Mohler JL, Kantoff PW, Armstrong AJ et al (2014) Prostate cancer, version 2.2014. *J Natl Compr Canc Netw* 12:686–718
4. Epstein JI (2006) What's new in prostate cancer disease assessment in 2006? *Curr Opin Urol* 16:146–151
5. Epstein JI, Allsbrook WC, Jr, Amin MB, Egevad LL, Committee IG (2005) The 2005 International Society of Urological Pathology (ISUP) Consensus Conference on Gleason Grading of Prostatic Carcinoma. *Am J Surg Pathol* 29:1228–1242
6. Gleason DF (1966) Classification of prostatic carcinomas. *Cancer Chemother Rep* 50:125–128
7. Gleason DF, Mellinger GT (1974) Prediction of prognosis for prostatic adenocarcinoma by combined histological grading and clinical staging. *J Urol* 111:58–64
8. Itou Y, Nakanishi K, Narumi Y, Nishizawa Y, Tsukuma H (2011) Clinical utility of apparent diffusion coefficient (ADC) values in patients with prostate cancer: can ADC values contribute to assess the aggressiveness of prostate cancer? *J Magn Reson Imaging* 33:167–172
9. Kobus T, Vos PC, Hambrock T et al (2012) Prostate cancer aggressiveness: in vivo assessment of MR spectroscopy and diffusion-weighted imaging at 3 T. *Radiology* 265:457–467
10. Vaché T, Bratan F, Mège-Lechevallier F, Roche S, Rabilloud M, Rouvière O (2014) Characterization of prostate lesions as benign or malignant at multiparametric MR imaging: comparison of three scoring systems in patients treated with radical prostatectomy. *Radiology* 272:446–455
11. Vargas HA, Akin O, Franiel T et al (2011) Diffusion-weighted endorectal MR imaging at 3 T for prostate cancer: tumor detection and assessment of aggressiveness. *Radiology* 259:775–784
12. Verma S, Rajesh A, Morales H et al (2011) Assessment of aggressiveness of prostate cancer: correlation of apparent

- diffusion coefficient with histologic grade after radical prostatectomy. *AJR Am J Roentgenol* 196:374–381
13. Litjens GJ, Barentsz JO, Karssemeijer N, Huisman HJ (2015) Clinical evaluation of a computer-aided diagnosis system for determining cancer aggressiveness in prostate MRI. *Eur Radiol* 25:318–3199
 14. Zhang YD, Wang Q, Wu CJ et al (2015) The histogram analysis of diffusion-weighted intravoxel incoherent motion (IVIM) imaging for differentiating the Gleason grade of prostate cancer. *Eur Radiol* 25:994–1004
 15. Zhou J, Blakeley JO, Hua J et al (2008) Practical data acquisition method for human brain tumor amide proton transfer (APT) imaging. *Magn Reson Med* 60:842–849
 16. Zhou J, Payen JF, Wilson DA, Traaystman RJ, van Zijl PC (2003) Using the amide proton signals of intracellular proteins and peptides to detect pH effects in MRI. *Nat Med* 9:1085–1090
 17. Togao O, Yoshiura T, Keupp J et al (2014) Amide proton transfer imaging of adult diffuse gliomas: correlation with histopathological grades. *Neuro Oncol* 16:441–448
 18. Dula AN, Arlinghaus LR, Dortch RD et al (2013) Amide proton transfer imaging of the breast at 3 T: establishing reproducibility and possible feasibility assessing chemotherapy response. *Magn Reson Med* 70:216–224
 19. Jia G, Abaza R, Williams JD et al (2011) Amide proton transfer MR imaging of prostate cancer: a preliminary study. *J Magn Reson Imaging* 33:647–654
 20. Tamada T, Sone T, Jo Y et al (2008) Prostate cancer: relationships between postbiopsy hemorrhage and tumor detectability at MR diagnosis. *Radiology* 248:531–539
 21. Keupp J, Baltes C, Harver P, Van den Brink J (2011) Parallel RF Transmission based MRI Technique for Highly Sensitive Detection of Amide Proton Transfer in the Human Brain at 3. In: Proceedings of 19th Annual Meeting of International Society of Magnetic Resonance in Medicine, Québec, p 710
 22. Agarwal HK, Keupp J, Bornardo M, Turkbey B, Choyke PL (2015) Saturation duration and power optimization for APT MRI of prostate cancer. In: Proceedings of 23rd Annual Meeting of International Society of Magnetic Resonance in Medicine, Toronto, p 3851
 23. Nagarajan R, Margolis D, Raman S et al (2012) MR spectroscopic imaging and diffusion-weighted imaging of prostate cancer with Gleason scores. *J Magn Reson Imaging* 36:697–703
 24. Oto A, Yang C, Kayhan A et al (2011) Diffusion-weighted and dynamic contrast-enhanced MRI of prostate cancer: correlation of quantitative MR parameters with Gleason score and tumor angiogenesis. *AJR Am J Roentgenol* 197:1382–1390
 25. Tamada T, Sone T, Jo Y et al (2008) Apparent diffusion coefficient values in peripheral and transition zones of the prostate: comparison between normal and malignant prostatic tissues and correlation with histologic grade. *J Magn Reson Imaging* 28:720–726
 26. Turkbey B, Shah VP, Pang Y et al (2011) Is apparent diffusion coefficient associated with clinical risk scores for prostate cancers that are visible on 3-T MR images? *Radiology* 258:488–495
 27. Donati OF, Mazaheri Y, Afaq A et al (2014) Prostate cancer aggressiveness: assessment with whole-lesion histogram analysis of the apparent diffusion coefficient. *Radiology* 271:143–152
 28. Mazaheri Y, Shukla-Dave A, Hricak H et al (2008) Prostate cancer: identification with combined diffusion-weighted MR imaging and 3D 1H MR spectroscopic imaging—correlation with pathologic findings. *Radiology* 246:480–488
 29. Wang XZ, Wang B, Gao ZQ et al (2009) Diffusion-weighted imaging of prostate cancer: correlation between apparent diffusion coefficient values and tumor proliferation. *J Magn Reson Imaging* 29:1360–1366
 30. Langer DL, van der Kwast TH, Evans AJ et al (2010) Prostate tissue composition and MR measurements: investigating the relationships between ADC, T2, K(trans), v(e), and corresponding histologic features. *Radiology* 255:485–494
 31. Tan CH, Wang J, Kundra V (2011) Diffusion weighted imaging in prostate cancer. *Eur Radiol* 21:593–603
 32. Zelfhof B, Pickles M, Liney G et al (2009) Correlation of diffusion-weighted magnetic resonance data with cellularity in prostate cancer. *BJU Int* 103:883–888
 33. Humphrey PA (2004) Gleason grading and prognostic factors in carcinoma of the prostate. *Mod Pathol* 17:292–306
 34. Nguyen K, Sarkar A, Jain AK (2014) Prostate cancer grading: use of graph cut and spatial arrangement of nuclei. *IEEE Trans Med Imaging* 33:2254–2270
 35. Freedland SJ, Kane CJ, Amling CL et al (2007) Upgrading and downgrading of prostate needle biopsy specimens: risk factors and clinical implications. *Urology* 69:495–499
 36. Sakr WA, Tefilli MV, Grignon DJ et al (2000) Gleason score 7 prostate cancer: a heterogeneous entity? Correlation with pathologic parameters and disease-free survival. *Urology* 56:730–734